FULL PAPER

Chemical shift encoding using asymmetric readout waveforms

Henric Rydén[1,2] (iD) | **Ola Norbeck**[1,2] (iD) | **Enrico Avventi**[1,2] (iD) | **Mikael Skorpil**[1,3] (iD) |
Adam van Niekerk[2] (iD) | **Stefan Skare**[1,2] (iD) | **Johan Berglund**[2] (iD)

[1]Department of Neuroradiology, Karolinska University Hospital, Stockholm, Sweden

[2]Department of Clinical Neuroscience, Karolinska Institutet, Stockholm, Sweden

[3]Department of Molecular Medicine and Surgery, Karolinska Institutet, Stockholm, Sweden

Correspondence
Henric Rydén, Department of
Neuroradiology, Karolinska University
Hospital, Eugeniavägen 11, B5:20, Solna
SE-171 76, Sweden.
Email: henric.ryden@ki.se

Purpose: To describe a new method for encoding chemical shift using asymmetric readout waveforms that enables more SNR-efficient fat/water imaging.

Methods: Chemical shift was encoded using asymmetric readout waveforms, rather than conventional shifted trapezoid readouts. Two asymmetric waveforms are described: a triangle and a spline. The concept was applied to a fat/water separated RARE sequence to increase sampling efficiency. The benefits were investigated through comparisons to shifted trapezoid readouts. Using asymmetric readout waveforms, the scan time was either shortened or maintained to increase SNR. A matched in-phase waveform is also described that aims to improve the SNR transfer function of the fat and water estimates. The sequence was demonstrated for cervical spine, musculoskeletal (MSK), and optic nerve applications at 3T and compared with conventional shifted readouts.

Results: By removing sequence dead times, scan times were shortened by 30% with maintained SNR. The shorter echo spacing also reduced T_2 blurring. Maintaining the scan times and using asymmetric readout waveforms achieved an SNR improvement in agreement with the prolonged sampling duration.

Conclusions: Asymmetric readout waveforms offer an additional degree of freedom in pulse sequence designs where chemical shift encoding is desired. This can be used to significantly shorten scan times or to increase SNR with maintained scan time.

KEYWORDS
chemical shift, Dixon, MRI

1 | INTRODUCTION

Fat tissue has special signal characteristics in MRI. In most sequences, fat is hyperintense due to its relatively short T_1, and low diffusivity compared to other soft tissues outside the brain. Due to chemical shift, fat is spatially shifted along the readout dimension. This bright and displaced signal can conceal pathology and decreases the dynamic range of the image. Several methods have been proposed to attenuate the fat signal. Although the physical rationale varies there are significant inefficiencies associated with each method.

The RF fat saturation technique employs a frequency selective RF pulse to excite only fat, followed by gradient spoiling to remove the signal prior to the main pulse sequence playout.[1,2] The fat saturation module is compatible with all pulse sequences, but has several drawbacks such as increased minimum TR, prolonged scan time, and decreased SNR efficiency. Besides these inefficiencies, the fat saturation technique fails in regions where the local off-resonance from field inhomogeneities exceeds the chemical shift, where it can instead suppress water signal.

The difference in T_1 relaxation times can, in combination with an inversion pulse and by synchronizing the excitation with the longitudinal zero-crossing of fat, be used to null the signal from fat.[3] This short tau inversion recovery (STIR) technique is insensitive to the local field inhomogeneity but incurs an inverted T_1-weighting, which may be undesirable. Since all tissues are subject to the inversion pulse, there is a significant and unavoidable SNR penalty. It is therefore often unfeasible to combine STIR with other inversion recovery techniques such as fluid attenuation (FLAIR). As opposed to chemical shift based methods, STIR is not molecule specific. Since tissues are suppressed merely on the basis of their T_1 relaxation times, STIR can suppress tissue with enough contrast uptake to mimic the T_1 of fat, counteracting the purpose of contrast administration.[4]

The Dixon methods use an assumed model of the signal where the fat and water component can be separated in the reconstruction process.[5] This puts requirements on the acquired signal. Typically, multiple echoes are acquired which prolongs the scan time. These additional chemical shift–encoded (CSE) echoes are, however, contributing to the signal in the reconstructed fat and water images, measured as an effective number of signal averages (NSA).[6] Theoretically, it has been shown that, with optimal sampling, the scan time penalty can be completely counterbalanced by the signal contribution from additional echoes.[7-10] The theoretical SNR efficiency of 100% is appealing, but hard to achieve in practice due to requirements specific to the pulse sequence, such as CPMG conditions. This defuses the major benefit of all acquired data contributing to the final image.

Earlier implementations of spin echo based Dixon methods share considerable downsides, resulting in an effective NSA lower than the number of echoes. The refocusing pulse cancels the chemical shift dephasing as the spin echo coincides with the center of the readout, rendering the inverse problem of separating fat and water ill posed. To enable CSE echoes in spin echo sequences the readout gradient is shifted from the center of the spin echo.[5,11,12] The technique of shifting readouts has also been applied to RARE[13] sequences, where three echo trains are played out, each with a unique shift of the readout gradient.[11] In order to fulfill CPMG conditions, the time between successive refocusing pulses must remain constant, and dead time is introduced to allow the desired CSE between every pair of refocusing pulses. For instance,

with 320 readout samples acquired with a receiver bandwidth (rBW) of ± 25 kHz/FOV, the readout window duration is 6.4 ms. To achieve a fat/water phase shift of π, 4.6/2.3 ms of dead time is required at 1.5/3 T, resulting in sampling occupancy of only 58/74%. Besides the inefficient sampling, the echo spacing is prolonged, resulting in stronger T_2 blurring.

An alternative to shifting echoes is to acquire multiple echoes between every pair of refocusing pulses[14] by applying readouts with alternating polarity, similar to GRASE,[15] but where the additional echoes encode chemical shift rather than phase encodes. Even if this does not introduce any dead time, the sequence is restricted to large echo spacings and an odd number of echoes in order to fulfill CPMG conditions, while only two echoes are required for fat/water separation. More importantly, in terms of sampling efficiency, all echoes acquired after the refocusing pulse have identical CSE to those prior, differing only in the angular direction of dephasing. This redundant sampling pattern negatively impacts the resulting NSA of the separated images.[7]

The inefficiencies of these RARE fat/water imaging methods might seem unrelated, but are a consequence of the readout waveforms being symmetrical. A GRASE readout block is symmetric around the spin echo, while the shifted readout is symmetric around its center of mass. In order to remove the redundant sampling of the GRASE readout block, at least one of the gradient lobes must differ from the rest, thus breaking the block symmetry. The shifted design requires additional echo spacing that cannot be used to acquire data since a prolonged readout is symmetric unless a partial Fourier acquisition is used, that is, *asymmetric sampling*. The latter method has been described by Ma et al,[16] but it is incompatible with undersampling along the phase encoding directions. The undersampling factor also varies between echoes, and requires special consideration to combine with fat/water separation in k-space.[17] A limiting factor of asymmetric sampling is also the largest possible dephasing time (time between gradient and spin echo), which is limited to half of the readout window duration. The technique is therefore best suited for low rBW acquisitions.

Recently, we described a two-point single-TR RARE sequence where readout asymmetry is achieved by employing two different readout amplitudes (dual bandwidths).[10] While an in-plane resolution of 0.5 mm was achieved at 3T, with a high-performance gradient system, resolutions beyond that are only feasible with a multi-TR acquisition. In this work, we propose using *asymmetric readout waveforms* to achieve efficient sampling with chemical shift encoding without dead time or redundancy. This technique allows for flexible echo shifts while still fulfilling CPMG conditions. The concept is applied to a RARE sequence to shorten scan time or to increase SNR. As a proof of concept, we also explore a modified symmetric in-phase waveform to improve chemical shift encoding.

2 | THEORY

2.1 | Designing the asymmetric waveform

The simplest asymmetrical waveform is the asymmetric triangle, described by the durations $T_{a,b}$, and slew rates $s_{a,b} = g/T_{a,b}$ of the two segments a and b shown in Figure 1A. The time-to-center, t_c, available acquisition time $T_{tot} = T_a + T_b$, and area M of the asymmetric triangle are given by the desired shift, echo spacing, and resolution, respectively. With the introduction of the auxiliary variable $T_1 = t_c - t_{as}$, the first segment duration T_a is equal to $2T_1^2/T_{tot}$ in the case of a positive shift. The triangle amplitude is $g = 2M/T_{tot}$. For a negative shift, the waveform is mirrored by swapping a and b.

The asymmetric triangle achieves a maximum positive shift when $T_b = 0$. Ignoring the infinite slew rate violation, a shift of only $T_{tot}\left(\sqrt{\frac{1}{2}} - \frac{1}{2}\right) \approx 0.2T_{tot}$ is achieved. This geometrical limitation causes the asymmetric triangle waveform to only be viable in sequence with long echo spacing.

To enable larger shifts, we designed a cubic spline-based waveform, shown in Figure 1B. As defined in the figure, the waveform is split into a trapezoidal base with amplitude g_0 and an asymmetric component. Sampling is started at t_{as}
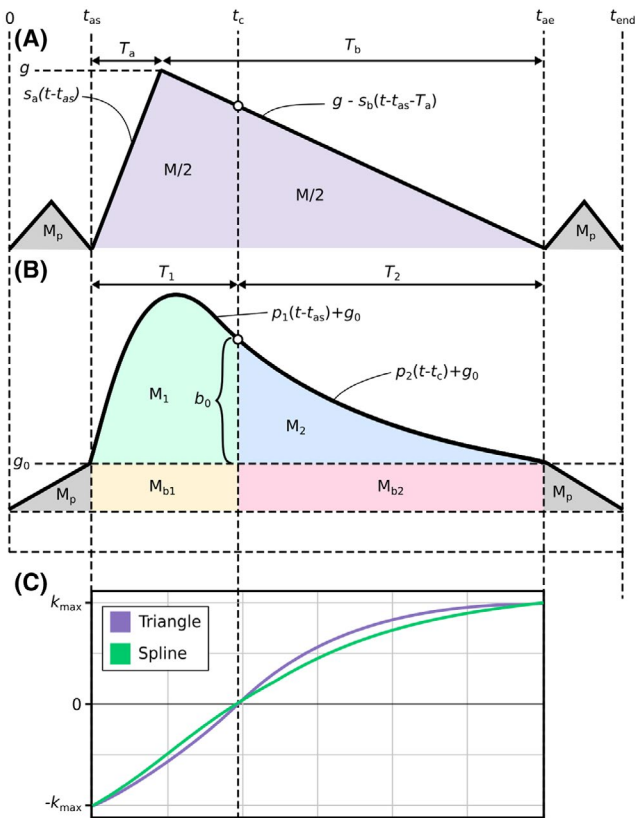

FIGURE 1 Asymmetric triangle (A) and spline (B) readout waveforms for chemical shift encoding. The k-space trajectory over time is shown in (C). The time axis (x) is shared between the plots

which is the instant at which the moment M_p is equal to the ramp area of the corresponding trapezoidal waveform. This is also the starting point of the first spline, p_1. The presampling duration t_{as} is known from the phase encoding or crusher gradient duration, whichever is longer. The base amplitude then follows as $g_0 = 2M_p/t_{as}$. With $T_2 = t_{ae} - t_c$, the base moments are simply $M_{b1} = g_0T_1$ and $M_{b2} = g_0T_2$.

Three knots are located at t_{as}, t_c, and t_{ae}, and the waveform is described by the two interval polynomials:

$$p_1(t) = \sum_{n=1}^{3} a_n t^n$$
$$p_2(t) = \sum_{n=0}^{3} b_n t^n \tag{1}$$

Further, p_1 and p_2 meet with C^2 continuity. In line with natural splines, $p_2''(T_2) = 0$. Given the desired center of mass at t_c the following must hold:

$$\int_0^{T_1} p_1(t)dt = M_1 = \frac{M}{2} - M_{b1} - M_p$$
$$\int_0^{T_2} p_2(t)dt = M_2 = \frac{M}{2} - M_{b2} - M_p \tag{2}$$

Finally, $p_2(T_2) = 0$, forming the exactly determined linear problem which can be written in matrix form as:

$$\begin{bmatrix} T_1 & T_1^2 & T_1^3 & -1 & 0 & 0 & 0 \\ 1 & 2T_1 & 3T_1^2 & 0 & -1 & 0 & 0 \\ 0 & 2 & 6T_1 & 0 & 0 & -2 & 0 \\ 0 & 0 & 0 & 0 & 0 & 2 & 6T_2 \\ T_1^2/2 & T_1^3/3 & T_1^4/4 & 0 & 0 & 0 & 0 \\ 0 & 0 & 0 & T_2 & T_2^2/2 & T_2^3/3 & T_2^4/4 \\ 0 & 0 & 0 & 1 & T_2 & T_2^2 & T_2^3 \end{bmatrix} \begin{bmatrix} a_1 \\ a_2 \\ a_3 \\ b_0 \\ b_1 \\ b_2 \\ b_3 \end{bmatrix} = \begin{bmatrix} 0 \\ 0 \\ 0 \\ 0 \\ M_1 \\ M_2 \\ 0 \end{bmatrix}. \tag{3}$$

The coefficients are available in the appendix. A consequence of enforcing the second derivative of p_2 to be zero at its endpoint is an undershoot in the waveform for positive shifts. This is avoided by calculating the waveform for a negative shift and then mirroring the result.

2.2 | Matching the in-phase echo

A property of the asymmetric readouts, resulting from the dynamic bandwidth, is the non-uniform k-space sampling density. We propose to counterbalance this with a matched in-phase readout to achieve a more balanced total k-space sampling density in a two-point RARE sequence. Ideally, the combined fat/water estimates will have an improved SNR transfer function with this approach (described below).

Although constrained to be symmetrical about the k-space origin, the sampling density of the matched readout can be varied. Instead of a conventional trapezoidal readout with fixed amplitude λ, we investigated a symmetric quadratic readout waveform which matches the CSE readout, illustrated

in Figure 2. $Q(t) = q_0 + q_2(t - t_{c,IP})^2$. The constant q_0 matches the asymmetric spline such that the combined effective dwell time at the k-space center equals that of two trapezoidal in-phase readouts. That is, the total time spent sampling the k-space center is the same: $\frac{1}{q_0} = \frac{2}{\lambda} - \frac{1}{b_0}$. The quadratic coefficient q_2 is defined by the gradient moment M, the center point $t_{c,IP}$ coinciding with the spin echo, and the constant q_0: $q_2 = \frac{3M}{2t_{c,IP}^3} - \frac{3q_0}{t_{c,IP}^2}$.

A comparison between the sampling densities for trapezoidal and quadratic in-phase readouts is shown in Figure 3. It is clear that while the density is non-uniform, the area is consistent between the spline, quadratic, and trapezoidal waveforms because the total readout durations are equal. In contrast, the shifted trapezoidal case shows a uniform distribution but with a smaller area. This is a consequence of less time spent sampling the signal. In Figure 4D, it is evident that the combined sampling time at the k-space center is increased and a more uniform density is achieved with the quadratic in-phase waveform. We hypothesize that the asymmetry of the sampling density can be counterbalanced by using real-valued k-space fat/water separation, described below.

3 | METHODS

3.1 | Pulse sequence

A RARE sequence was implemented that alternates the acquisition of in and opposed phase echoes between excitations, as shown in Figure 4. All waveform calculations were calculated on-the-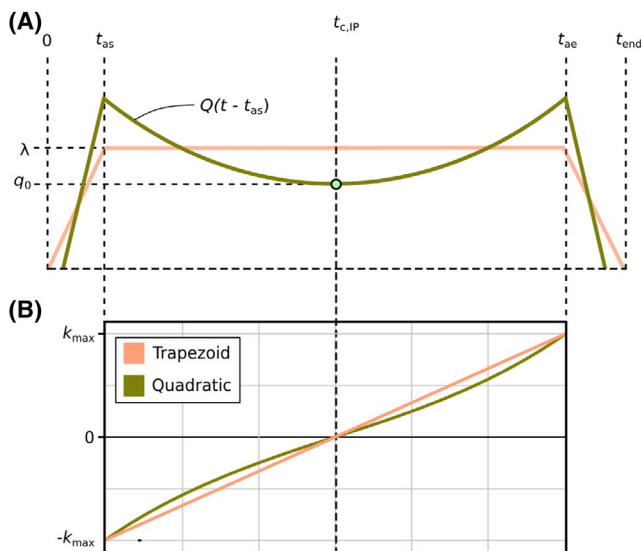fly, without delay, according to the prescribed scan parameters. The CSE echo was acquired with the spline waveform, while the in-phase echo was acquired with a quadratic readout, shown in Figure 2 and described in more detail below. The conventional trapezoid was compared against the quadratic.

Samples were acquired with a constant minimum receiver dwell time (2 μs), using as wide an analog filter bandwidth as possible. A sinc-based Cartesian gridding procedure[18] was applied with matched filter design to equalize the signal variance.[19] The signal power is related to the sampling density, described by the square root of the sinc integral, $\sqrt{\tau}$. τ can be interpreted as the effective dwell time of a gridded sample. The white noise resampling procedure was chosen over uniform signal in order to facilitate apparent SNR measurements in the resampled images. An example of the sampling density is shown in Figure 4. Since the regridding is a one-dimensional problem and the trajectories are monotonic, fully supported sinc functions are computationally feasible. This also avoids deapodization.

3.2 | Fat/water separation

The matched filter resampling procedure equalizes noise in the gridded domain. However, this results in fluctuations in the signal intensity that is proportional to the sampling density, or effective dwell time τ. This can be incorporated into the signal model as follows:

$$\underbrace{\begin{bmatrix} S_1 \\ S_2 \end{bmatrix}}_{S} = e^{i\phi} \underbrace{\begin{bmatrix} e^{i\psi t_1} & 0 \\ 0 & e^{i\psi t_2} \end{bmatrix}}_{B(\psi)} \underbrace{\begin{bmatrix} \sqrt{\tau_1} & 0 \\ 0 & \sqrt{\tau_2} \end{bmatrix}}_{\Lambda} \underbrace{\begin{bmatrix} 1 & a_1 \\ 1 & a_2 \end{bmatrix}}_{A} \underbrace{\begin{bmatrix} W \\ F \end{bmatrix}}_{x},$$

(4)

where ϕ describes the initial phase after excitation, calculated as described by Berglund et al.[20] Equation (4) accounts for multiple fat peak resonances ω with relative weights α[21]: $a_n = \sum_{p=1}^{P} \alpha_p e^{i\omega_p t_n}$. Non-chemical shift off-resonances ψ are determined with a multiscale graph cut technique.[22]

Since **S** is acquired with different gradient strengths, not only between samples but also between echoes, the chemical shift displacement can lead to unfamiliar artifacts. This frequency-dependent blurring can be corrected for by solving for **x** in k-space.[17]

By modeling **x** as real-valued in image space, fat and water estimation enforces conjugate symmetry in k-space.[20] Although Equation (4) is exactly determined (two complex measurements S_1, S_2, and four real-valued estimates, ϕ, ψ, W, and F), estimating and demodulating only low resolution ϕ- and ψ-maps leaves an over-determined inverse problem. The additional degrees of freedom can be used to take advantage of the known differences in signal uncertainties **Λ** for an improved estimation:

FIGURE 2 Symmetric readout waveforms for in-phase CSE. A trapezoid and the proposed matched quadratic waveform is shown in (A). The k-space trajectory over time is shown in (B). The time axis (x) is shared between the plots
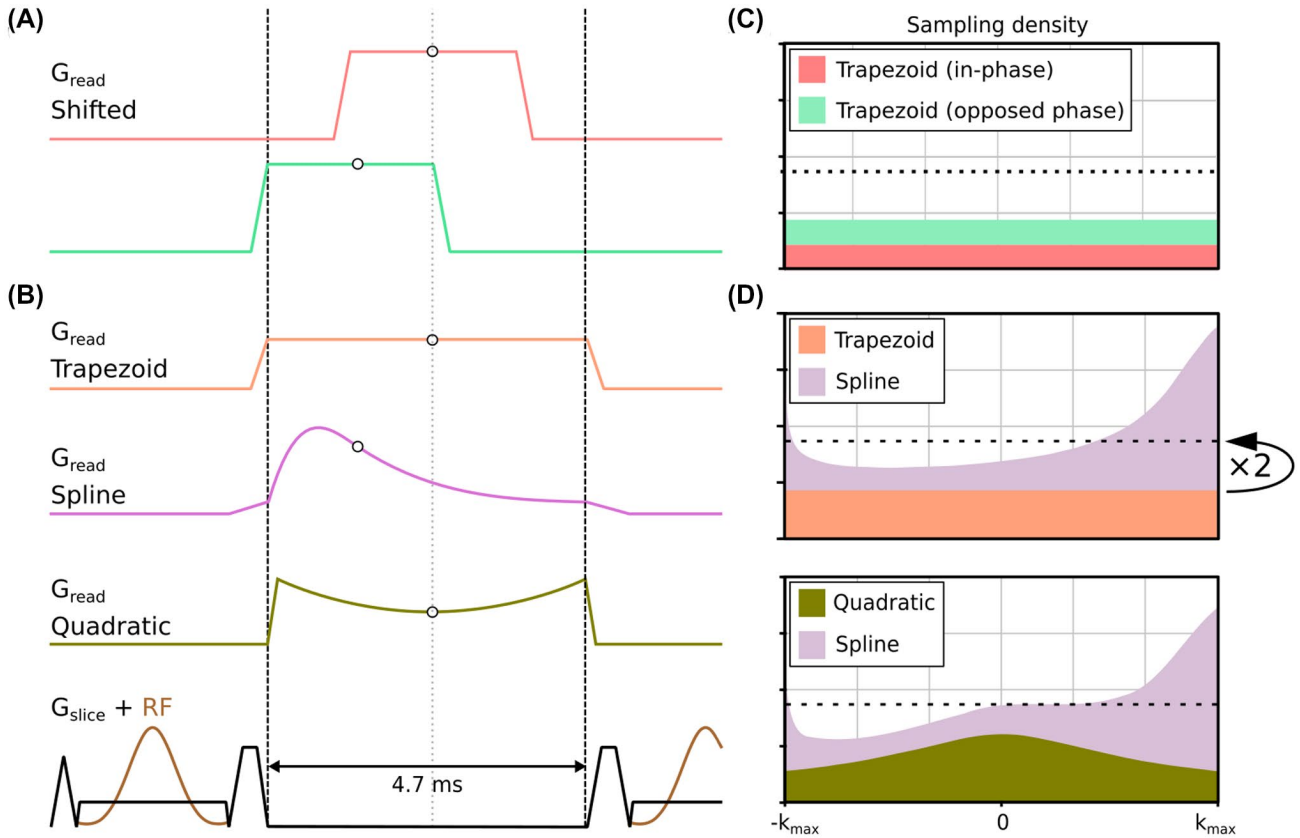
FIGURE 3 A, Conventional multi-TR RARE imaging where the readouts are shifted according to the desired CSE, prolonging the echo spacing. The dead times are avoided in (B) where asymmetric readout waveforms are used for CSE. The middle rows in (B) show the two investigated in-phase alternatives: quadratic and prolonged trapezoidal readouts. Shaded areas indicate sampling

$$\mathcal{F}(\hat{\mathbf{x}})_k = \underbrace{\begin{bmatrix} (\mathbf{\Lambda A})_k \\ (\mathbf{\Lambda A})_c^* \end{bmatrix}}_{\mathbf{E}}^{\ddagger} \begin{bmatrix} \mathcal{F}(\mathbf{S}^{\phi,\psi})_k \\ \mathcal{F}(\mathbf{S}^{\phi,\psi})_c^* \end{bmatrix} \quad (5)$$

Here, $\mathcal{F}()$ is the Fourier transform operator, and $S^{\phi,\psi} = Se^{-i(\hat{\phi}+\hat{\psi}t)}$ denotes an acquired echo after image space demodulation with the estimated $\hat{\phi}$ and $\hat{\psi}$. The * superscript indicates the complex conjugate. The encoding matrix $(\mathbf{\Lambda}A)_k$ for sample k is stacked with that of its conjugate sample c, that is, the point mirrored around the k-space center. A Tikhonov regularization is applied to the pseudo inverse to reduce colored noise,[23] indicated by \ddag. The regularization term is chosen to equalize the noise power spectrum (NPS) of the *combined* fat and water estimates as previously described.[24] This forms the noise-whitening weighted least squares estimator $\mathbf{E}^{\ddagger}$.

The NPS of water and fat can be extracted from the diagonal elements of $\mathbf{E}^{\ddagger}(\mathbf{E}^{\ddagger})^H$, where $(\mathbf{E}^{\ddagger})^H$ is the conjugate transpose of $\mathbf{E}^{\ddagger}$. The modulation transfer function (MTF) describes the frequency loss in the estimates, and can be calculated from the diagonal elements of $\mathbf{E}^{\ddagger}\mathbf{E}$. A theoretical SNR transfer function for $\hat{\mathbf{x}}_k$ can be calculated from the ratio between the corresponding MTF and NPS.

3.3 | Data acquisition

Informed consent was obtained from all three volunteers (male, age 29, 33, and 48) in accordance with the institutional review board policy. All images were acquired on a 3T Signa Premier (GE Healthcare). Phase encoding line synthesization was implemented using GRAPPA.[25] Relevant scan parameters are listed in Table 1.

High-resolution PD-weighted images of the foot and knee were acquired with dedicated Rx and Tx/Rx coils, respectively. The in-phase echo was acquired with the matched quadratic waveform.

Sagittal T_2-weighted images of the cervical spine were acquired with the conventional shifted approach. The sampling duration was kept constant but the echo spacing was shortened by employing the spline waveform for an opposed phase CSE. The echo train length was increased to achieve the same effective echo time, thereby reducing the scan time. We also acquired images using the matched quadratic in-phase waveform.

The recently described single-TR dBW-RARE technique[10] was compared against the proposed multi-TR RARE sequence. As the multi-TR sequence has twice as long

FIGURE 4 Sampling densities and waveforms in a RARE pulse sequence. The G_{slice} + RF row shows the slice selection gradient and refocusing RF pulses for a scan with t_{tot} = 4.7 ms. (A) Conventional shifted trapezoids with dead times. (B) Trapezoidal, spline, and matched quadratic waveforms. The sampling density, is shown as stacked plots in (C) and (D). The quadratic in-phase waveform more densely samples the k-space center, contributing to a more leveled combined sampling density. A reference line (dashed) shows the sampling density achieved by two prolonged trapezoids. By design, the density with the quadratic and spline waveform hits this line at the k-space center
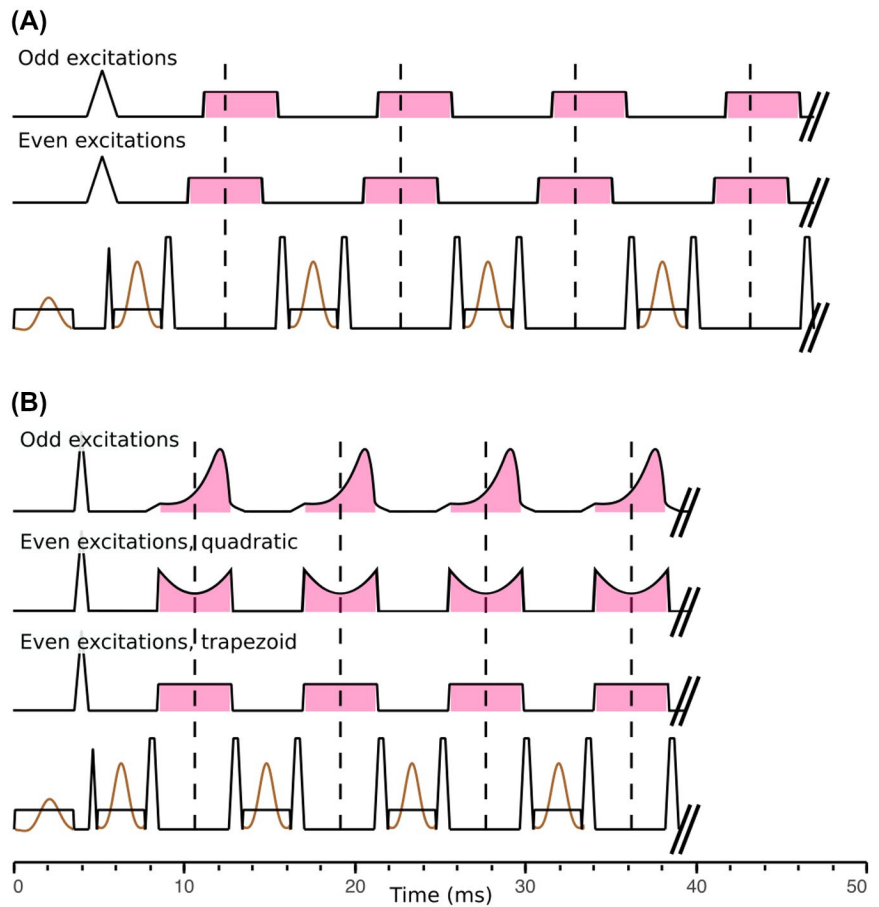

TABLE 1 Acquisition parameters

Description	C-Spine	Knee	Foot	Single-TR comparison	SNR
	Shifted/Asymmetric			dBW/Asymmetric	
Echo train length	12/16	7	7	6	12
FOV (F × P, mm)	220 × 220	140 × 140	240 × 360	160 × 160	220 × 220
TR (ms)	3000	3000	3000	3500	3000
TE (ms)	81/83	42	42	33	83
Pixel size (mm)	0.7 × 0.7	0.3 × 0.3	0.5 × 0.5	0.6 × 0.6	0.7 × 0.7
Slice thickness (mm)	4	2.5	2.5	2	3
T_{tot} (ms)	5.12	4.49	4.49	3.84	7.12
CSE (ms)	−1.0	−1.0	−1.0	(−0.2, 1.2)/−1.1	−1.0
Peak slew rate (T/m/s)	29	115	65	146/115	9
Acquisition time (m:s)	2:42/1:57	3:12	5:03	2:51/3:05	2 × 2:43
Figure number	5	6	7	8	9
R (GRAPPA)	2	2	1	1/2	1

Note: Acquisition time was doubled for the SNR measurements to estimate noise.

acquisition time, which also benefits the SNR, the scan time was matched using in-plane GRAPPA acceleration. However, as GRAPPA requires reference lines, the scan time was slightly longer with the proposed technique. The partial Fourier fraction with dBW-RARE was 0.75.

The use of an asymmetric readout gradient can also be used to allow more sampling for a fixed echo spacing. We therefore compared the SNR impact on this increased sample duration and compared it to the shifted approach. The SNR impact of a matched quadratic in-phase waveform was also investigated.
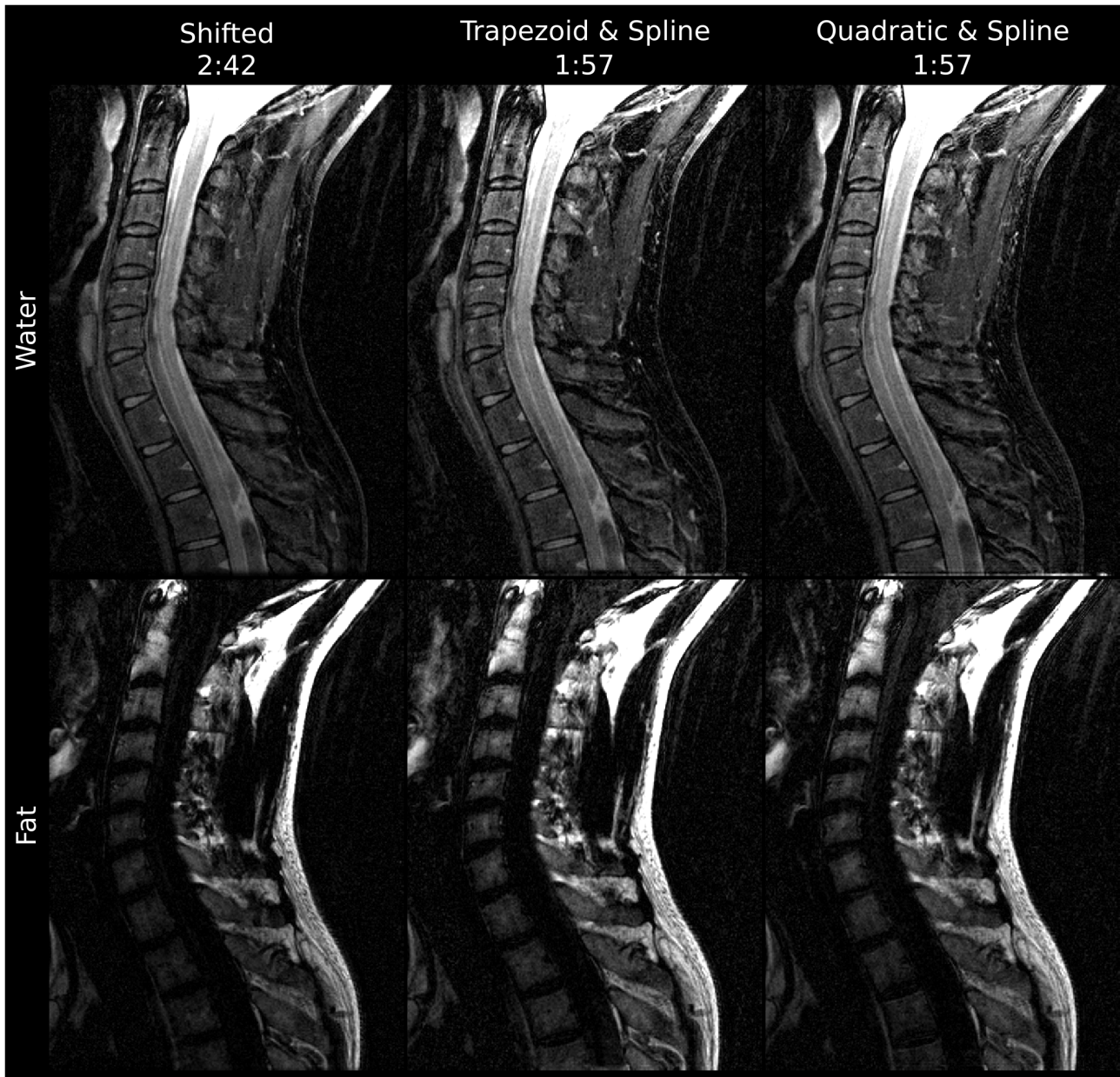
FIGURE 5 Cervical spine where the asymmetric readouts are used to shorten scan time. While the image quality is comparable, the scan time is 38% longer for the shifted acquisition. Similar image quality is seen with the quadratic in-phase waveform

T_2-weighted images of the optic nerve were also acquired. SNR maps were generated as described previously,[10] with regions of interests placed to avoid bias from flow artifacts. The apparent SNR was measured by acquiring each phase encoding line twice, thus doubling the scan time. Note that these apparent SNR measurements are almost entirely determined by the SNR at the center of k-space, as the majority of the signal originates there and the method for measuring it involves smoothing.[26] A measurement of apparent SNR is therefore highly dependent on the effective dwell time of the k-space center, which varies significantly between the different waveforms. Additionally, with the decision to whiten noise in order to facilitate apparent SNR measurements, the in- and opposed

phase images are filtered differently. Compared to a uniform signal resampling, the matched quadratic in-phase signal is in general more low-pass filtered and the opposed phase signal is more high-pass filtered. This does not affect the estimates as this is incorporated in Equation (4). For the full picture, the SNR transfer function describes the expected SNR for all spectral components.

3.4 | Supplementary material

An online GitHub repository is provided with interactive plots of the proposed waveforms at henricryden.github.io/
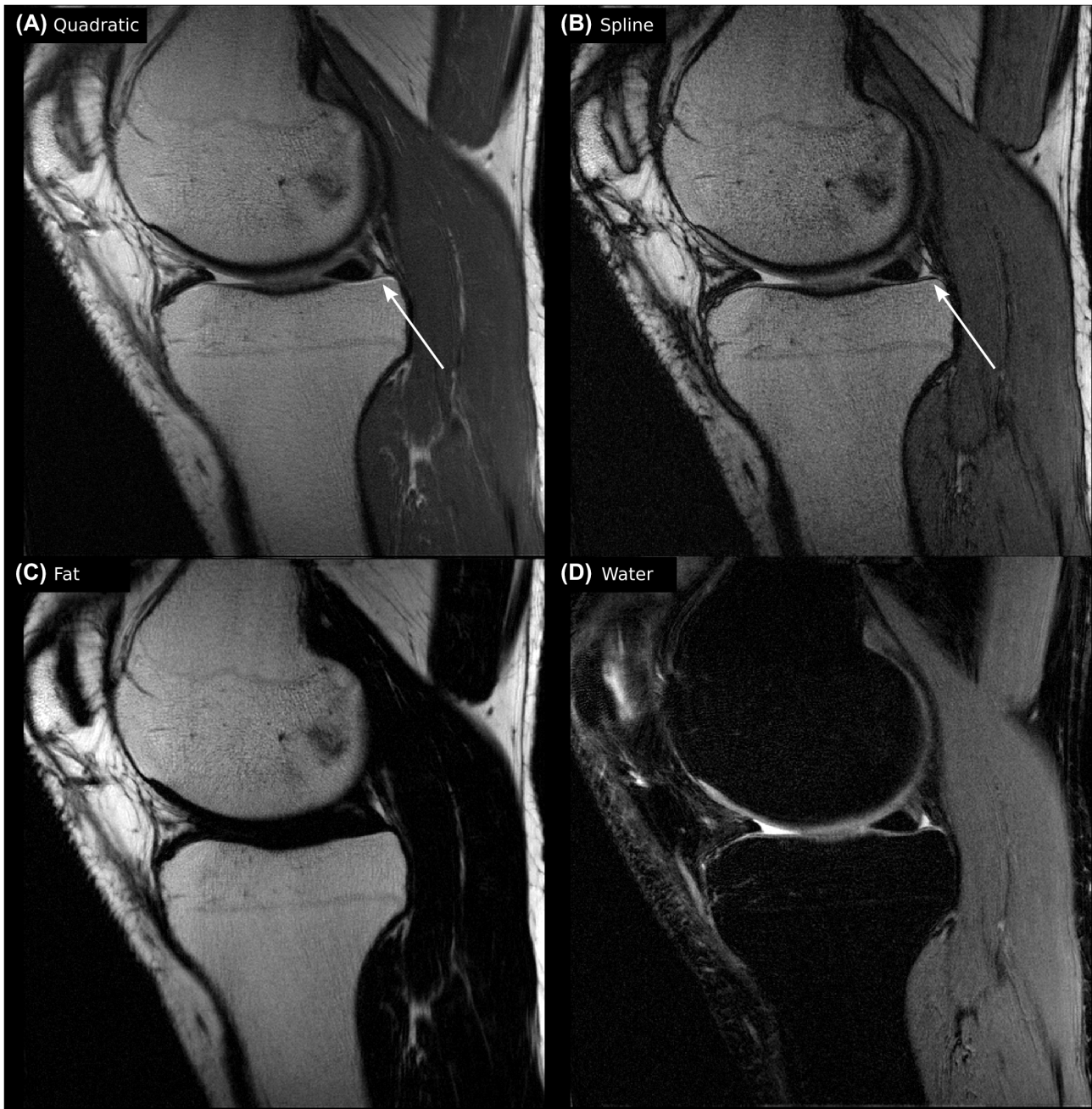
FIGURE 6 Sagittal knee images acquired with quadratic (A) and spline (B) readout waveforms. Signal pile-up from chemical shift displacement is indicated by white arrows, which are more pronounced in (A) compared to (B). This artifact is removed in (C) and (D) by performing the separation in k-space and modeling the k-space trajectory

asymreadout, where the user can see set scan parameters and the waveforms and sampling density are updated interactively. A complete interactive plot of the RARE pulse sequence is also available.

4 | RESULTS

Sagittal T_2-weighted fat/water images of the cervical spine are shown in Figure 5. In this case, shifted trapezoids prolong the echo spacing by 38%. This is avoided with asymmetric readouts. The proposed matched quadratic in-phase waveform is also shown. Fat and water is successfully separated in both cases, and similar image quality is obtained.

The PD-weighted sagittal knee images in Figure 6 reveal fine anatomical details in both the acquired echoes and the estimated fat and water images. Chemical shift displacement can be seen, which manifests more strongly in the quadratic in-phase echo, due to the lower bandwidth when acquiring the center of k-space. The tibial bone marrow fat is displaced,

superimposing on the cartilage which makes it indiscernible at some regions in the native images. However, the cartilage is clearly seen in the water image, and easily distinguished from the adjacent synovial fluid which appears brighter. The displacement correction is achieved by accounting for the dephasing times of each sample in Equation (5). The opposed phase image acquired with the spline waveform has a sampling density that emphasizes high spatial frequencies. While a higher noise level can be seen in homogeneous regions such as in the muscles, the trabecular structures, and remnant of epiphyseal plates are more strongly depicted.

Enhanced bone structures are also seen in the opposed phase image in Figure 7. Successful suppression of the fat allows a clear depiction of the cartilage across the entire field of view.

The comparison between dBW-RARE and the asymmetric encoding is shown in Figure 8.

Results from the apparent SNR measurements are shown in Figure 9. Although affected by eye motion induced artifacts, fat and water were successfully separated in all acquired slices. Compared to shifted trapezoids, an improved apparent SNR of 20% was obtained with the prolonged trapezoid, and a smaller improvement of 2-3% with the spline. The matched quadratic in-phase waveform has an improved apparent SNR of 34%. The separated fat and water estimates have higher apparent SNR when using the quadratic in-phase waveform. The SNR transfer function derived from the encoding matrices is also shown. At the k-space center (vertical dashed line), the theoretical SNR is higher than with a shifted acquisition, in-line with the apparent SNR measurements. The overall improvement in SNR across k-space is an effect from the increase in sampling duration.

5 | DISCUSSION

Here, we describe a new way of encoding chemical shift with variable density along the readout dimension. More specifically, the encoding is asymmetric to a degree required to achieve the desired CSE. Variable density sampling is commonly used in non-Cartesian sequences, for example, in spiral imaging to reduce aliasing artifacts[27] or for the reduction of
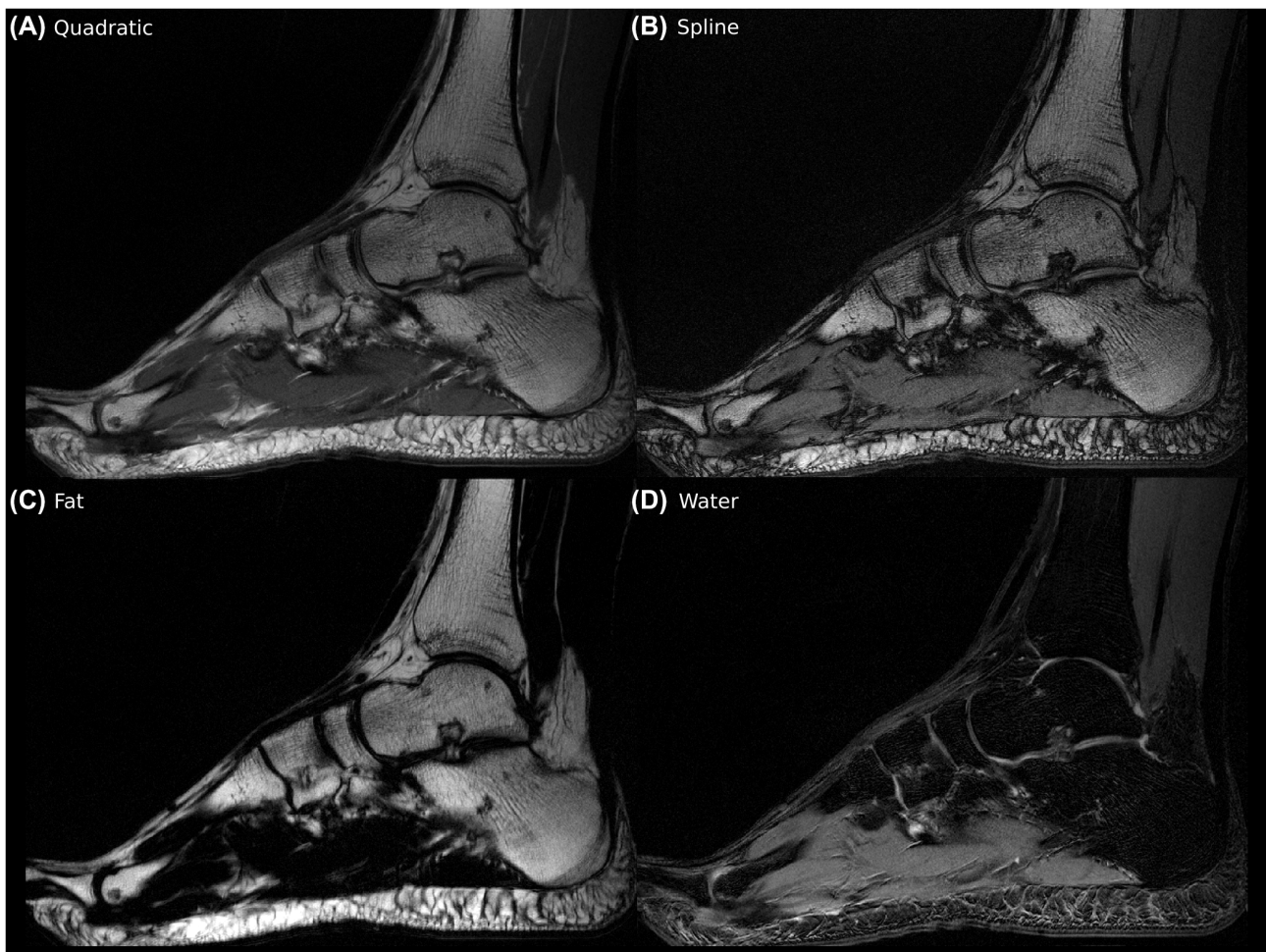

FIGURE 7 PD-weighted sagittal foot acquired at 3T. Cartilage structures are well separated from the bone marrow in the water image (D). Trabecular structures are enhanced in (B)
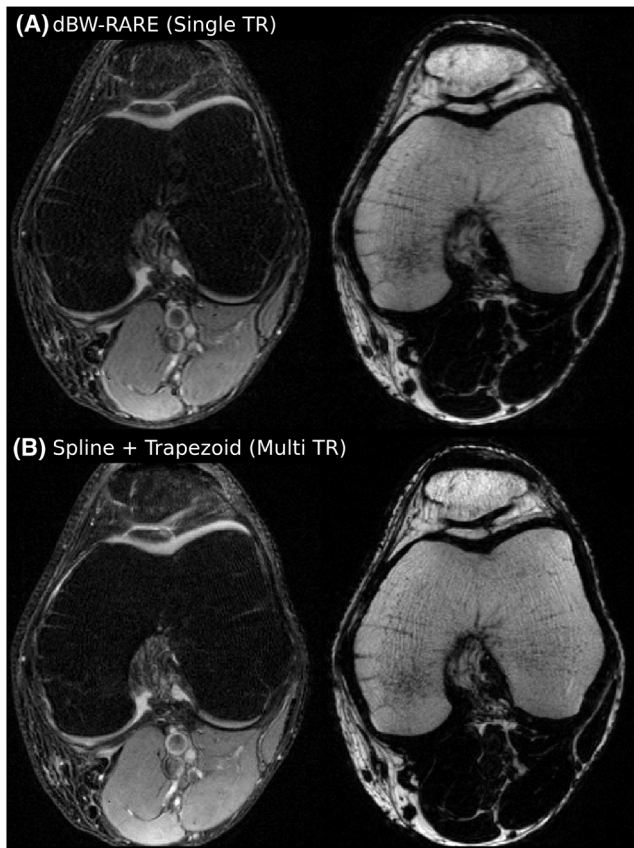
FIGURE 8 Comparison between the single-TR dBW-RARE sequence (A) and the proposed multi-TR RARE sequence (B). Water and fat images are shown to the left and right, respectively. The acquisition time was matched by using in-plane acceleration ($R = 2$) in (B)

spectral side-lobes in spiral CSI.[28] Irregular phase encoding sampling can be applied to Cartesian imaging to shorten scan times[27,29] at the cost of high frequency aliasing. It is possible to remove this artifact using GRAPPA to synthesize missing lines. Randomly undersampling phase encodes also shorten scan times, and can be reconstructed with compressed sensing techniques.[30] Variable density sampling along frequency encoding is common practice in EPI to reduce echo spacing by ramp sampling. With a priori knowledge of the smoothing procedure in fMRI, the sampling can be optimized in both directions to optimize BOLD sensitivity.[19] Contrary to the phase encoding techniques mentioned above, the Nyquist criterion is still fulfilled with the proposed technique as the ADC can sample more densely without a scan time penalty.

Single-TR methods for Dixon RARE imaging are mainly restricted by gradient performance as multiple echoes are acquired between refocusing pulses. For the well-established fast triple echo Dixon technique (fTED,[16]), T_{tot} is fixed to two periods of fat dephasing, that is, 9.2/4.6 ms at 1.5/3T. Although more recently, fTED with flexible shifts has been described,[31] this comes at the cost of lower effective NSA as the CSE echoes are not acquired exactly opposed phase.[7]

Even with a high-performance gradient system, readout resolutions higher than about 1 mm are not achievable with conventional fTED at 3T. By only encoding two echoes with different bandwidths and partial Fourier sampling, we recently reported readout resolutions of 0.5 mm at 3T.[10]

Multi-TR acquisitions, on the other hand, do not have a resolution restriction as only one echo is acquired during T_{tot}, allowing much larger k-space coverage. The downside of multi-TR is the increased scan time, and dead times arising from the shifts, resulting in a more than twofold increase in scan time compared to single-TR acquisitions. The additional excitations contribute to the signal and can be compensated by other acceleration techniques, including reduced phase field of view, decreased NSA, partial Fourier, or parallel imaging. Dead times, however, increase the scan time without SNR benefits. By using asymmetric readout waveforms, these dead times are avoided, thereby reducing scan time and echo spacing. A 38% scan time penalty is reported with the shifted readouts in Figure 5, and would be twice as much at 1.5 T-given the same scan parameters—since the chemical shift dephasing period and hence the dead times for the shifted acquisitions are doubled. It should be noted that non-Cartesian sequences such as time offset spirals do not suffer from these large dead times as the readout is much longer.[32]

The comparison with dBW-RARE in Figure 9 shows a sharper fat image with the proposed technique and less artifacts. These artifacts in dBW-RARE are likely attributed to the partial Fourier sampling. This comparison is, however, somewhat unfair as the dBW-RARE sequence struggles with such short acquisition windows and with the resolution pushed to its limit.

Chemical shift displacement artifacts are seen in all acquired echoes in Figure 9, but less pronounced in the spline images than in the quadratic in-phase images. An apparent SNR improvement is seen with the quadratic waveform. These effects are expected since, by design, the quadratic waveform has a lower bandwidth at the acquisition of k-space center. The reported apparent SNR increase of 14% is in line both with the expected SNR gain of 17% from the prolonged sampling duration and that calculated from the SNR transfer function at the k-space center. This SNR improvement would require 30% longer scan time with shifted readouts. It should be emphasized that the gain in SNR of the proposed technique is sourced from the additional sampling duration, which results in an SNR gain for almost all spectral components as evident from the SNR transfer function. The measured apparent SNR is almost entirely governed by the effective dwell time at the k-space center. A comparison of apparent SNR between acquired echoes is therefore difficult to make due to different resampling filters. The full picture is given by the SNR transfer function, and the apparent SNR measurements should be considered as an in-vivo validation at the center frequency.
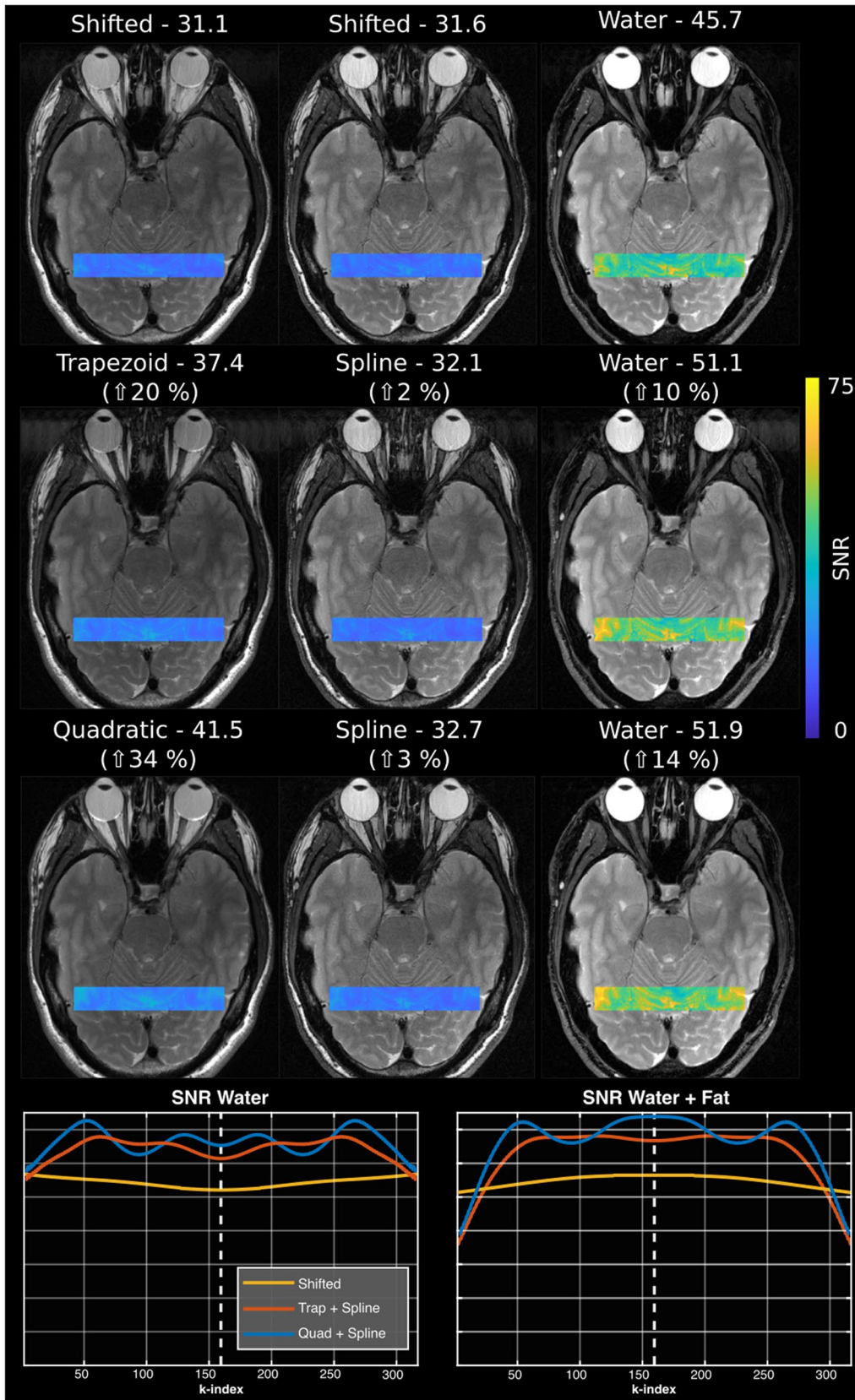
FIGURE 9 Apparent SNR comparison of the spline, prolonged trapezoid, and quadratic echoes together with their water estimates. The first column shows images from the three in-phase waveforms. The second column shows opposed phase images. Reconstructed water images are seen in the third column. All images have a colored region showing the measured apparent SNR, with its average value reported in the figure. The bottom rows show the theoretical SNR transfer function of each k-space index, derived from the encoding matrices

The spline waveform was designed to achieve the desired shift for a given available acquisition time T_{tot}. This typically results in a decreased effective dwell time at the k-space center and more time spent sampling higher spatial frequencies. Even though the apparent SNR does not increase even though the total sample duration does, the high frequency content should be more well resolved. This is supported by the clearer depiction of finer structures in Figures 6 and 7 compared to the in-phase images.

The set of dephasing times for k-space center acquisition is determined by the desired shift, while the first and last sample pair will always have identical CSE. Consequently, **A** is singular at the edges of k-space, and while Hermitian symmetry will improve conditionality in general, the conjugate operator in Equation (5) results in **E** being rank deficient. This en passant discovery is intuitive in hindsight, because there is no CSE resolved in the four samples.

Another interesting encoding property arises from the varying sample density (Figure 4), which in combination with varying dephasing times, results in a non-uniform SNR transfer function (Figure 9). The quadratic waveform increases the SNR at the k-space center, which is reflected in the apparent SNR measured in vivo. At the outer samples, the encoding is inferior but this is partly alleviated, for some indices, by the conjugate sample. The real-valued estimates also make the SNR transfer function symmetric. Moreover, water is less affected than the combined estimates in terms of the SNR transfer function and both proposed sequences outperform the shifted alternative in this work.

In Dixon imaging, the fat image can serve as a T_1-weighted surrogate that discriminates between tissue types.[33] The improved sharpness in the opposed phase image reported here enhances the trabecular bone structures, and complements the tissue-classifying fat/water images. The opposed phase image might therefore be of value in evaluating fractures and trabecular destruction, similar to previous works.[34,35] With the correction of chemical shift displacement, we expect simpler evaluation of cartilage thickness.

Chemical shift encoding can be achieved by any asymmetric readout gradient. Other readout waveforms such as a piece-wise linear shape, or an asymmetric triangle stacked on a rectangular base, would be of interest to explore. The waveforms described in this work were designed by only considering the conditioning of the k-space center, and it is expected that other more precisely tailored waveforms can achieve a further improved SNR transfer function. The quadratic waveform shows that the SNR transfer function can be modified by also considering the in-phase waveform, although it must be symmetric. More work can also be done on the regularization to yield optimized fat and water images, as opposed to the current technique where the noise amplification factor considers the *sum* of *W* and *F*.

6 | CONCLUSION

Asymmetric readout waveforms can be used as an alternative to shifted trapezoids to encode chemical shift, enabling more efficient Dixon imaging. This allows for significant scan time reduction, increased SNR, or a combination thereof in RARE sequences. By removing sequence dead times, the echo spacing is also shortened, reducing T_2 blurring. The variable sampling density can be accounted for in the fat/water separation, and further compensated by also modifying the in-phase waveform to achieve a more uniform SNR transfer function.

ORCID
Henric Rydén https://orcid.org/0000-0003-3269-7482
Ola Norbeck https://orcid.org/0000-0002-0518-5206
Enrico Avventi https://orcid.org/0000-0003-1000-6134
Mikael Skorpil https://orcid.org/0000-0002-2759-4692
Adam van Niekerk https://orcid.org/0000-0001-9731-6930
Stefan Skare https://orcid.org/0000-0001-5403-2153
Johan Berglund https://orcid.org/0000-0002-0853-9305

REFERENCES
1. Rosen BR, Wedeen VJ, Brady TJ. Selective saturation NMR imaging. *J Comput Assist Tomogr*. 1984;8:813-818.
2. Haase A, Frahm J, Hänicke W, Matthaei D. ^{1}H NMR chemical shift selective (CHESS) imaging. *Phys Med Biol*. 1985;30:341-344.
3. Bydder GM, Young IR. MR imaging: clinical use of the inversion recovery sequence. *J Comput Assist Tomogr*. 1985;9:659-675.
4. Krinsky G, Rofsky NM, Weinreb JC. Nonspecificity of short inversion time inversion recovery (STIR) as a technique of fat suppression: pitfalls in image interpretation. *Am J Roentgenol*. 1996;166:523-526.
5. Dixon WT. Simple proton spectroscopic imaging. *Radiology*. 1984;153:189-194.
6. Glover GH. Multipoint Dixon technique for water and fat proton and susceptibility imaging. *J Magn Reson Imaging*. 1991;1:521-530.
7. Pineda AR, Reeder SB, Wen Z, Pelc NJ. Cramér-Rao bounds for three-point decomposition of water and fat. *Magn Reson Med*. 2005;54:625-635.
8. Eggers H, Brendel B, Duijndam A, Herigault G. Dual-echo Dixon imaging with flexible choice of echo times. *Magn Reson Med*. 2011;65:96-107.
9. Berglund J, Ahlström H, Johansson L, Kullberg J. Two-point Dixon method with flexible echo times. *Magn Reson Med*. 2011;65:994-1004.
10. Rydén H, Berglund J, Norbeck O, et al. RARE two-point Dixon with dual bandwidths. *Magn Reson Med*. 2020;84:2456–2468. https://doi.org/10.1002/mrm.28293
11. Hardy PA, Hinks RS, Tkach JA. Separation of fat and water in fast spin-echo MR imaging with the three-point Dixon technique. *J Magn Reson Imaging*. 1995;5:181-185.

12. Glover GH, Schneider E. Three-point dixon technique for true water/fat decomposition with B_0 inhomogeneity correction. *Magn Reson Med*. 1991;18:371-383.

13. Hennig J, Nauerth A, Friedburg H. RARE imaging: a fast imaging method for clinical MR. *Magn Reson Med*. 1986;3:823-833.

14. Ma J, Son JB, Zhou Y, LePetross H, Choi H. Fast spin-echo triple-echo dixon (fTED) technique for efficient T_2-weighted water and fat imaging. *Magn Reson Med*. 2007;58:103-109.

15. Oshio K, Feinberg DA. GRASE (gradient- and spin-echo) imaging: a novel fast MRI technique. *Magn Reson Med*. 1991;20:344-349.

16. Ma J, Singh SK, Kumar AJ, Leeds NE, Broemeling LD. Method for efficient fast spin echo Dixon imaging. *Magn Reson Med*. 2002;48:1021-1027.

17. Brodsky EK, Holmes JH, Yu H, Reeder SB. Generalized k-space decomposition with chemical shift correction for non-cartesian water-fat imaging. *Magn Reson Med*. 2008;59:1151-1164.

18. O'Sullivan JD. A fast sinc function gridding algorithm for fourier inversion in computer tomography. *IEEE Trans Med Imaging*. 1985;4:200-207.

19. Kasper L, Haeberlin M, Dietrich BE, et al. Matched-filter acquisition for BOLD fMRI. *Neuroimage*. 2014;100:145-160.

20. Berglund J, Rydén H, Avventi E, Norbeck O, Sprenger T, Skare S. Fat/water separation in k-space with real-valued estimates and its combination with POCS. *Magn Reson Med*. 2020;83:653-661.

21. Yu H, Shimakawa A, McKenzie CA, Brodsky E, Brittain JH, Reeder SB. Multiecho water-fat separation and simultaneous R_2^* estimation with multifrequency fat spectrum modeling. *Magn Reson Med*. 2008;60:1122-1134.

22. Berglund J, Skorpil M. Multi-scale graph-cut algorithm for efficient water-fat separation. *Magn Reson Med*. 2017;78:941-949.

23. Lu W, Yu H, Shimakawa A, Alley M, Reeder SB, Hargreaves BA. Water-fat separation with bipolar multiecho sequences. *Magn Reson Med*. 2008;60:198-209.

24. Rydén H, Berglund J, Norbeck O, Avventi E, Skare S. T_1 weighted fat/water separated PROPELLER acquired with dual bandwidths. *Magn Reson Med*. 2018;42:963.

25. Griswold MA, Jakob PM, Heidemann RM, et al. Generalized autocalibrating partially parallel acquisitions (GRAPPA). *Magn Reson Med*. 2002;47:1202-1210.

26. Steckner MC, Liu B, Ying L. A new single acquisition, two-image difference method for determining MR image SNR. *Med Phys*. 2009;36:662-671.

27. Tsai CM, Nishimura DG. Reduced aliasing artifacts using variable-density k-space sampling trajectories. *Magn Reson Med*. 2000;43:452-458.

28. Adalsteinsson E, StarLack J, Meyer CH, Spielman DM. Reduced spatial side lobes in chemical-shift imaging. *Magn Reson Med*. 1999;42:314-323.

29. Marseille GJ, de Beer R, Fuderer M, Mehlkopf AF, van Ormondt D. Nonuniform Phase-Encode distributions for MRI scan time reduction. *J Magn Reson B*. 1996;111:70-75.

30. Lustig M, Donoho D, Pauly JM. Sparse MRI: the application of compressed sensing for rapid MR imaging. *Magn Reson Med*. 2007;58:1182-1195.

31. Son JB, Hwang KP, Madewell JE, et al. A flexible fast spin echo triple-echo dixon technique. *Magn. Reson. Med*. 2017;77:1049-1057.

32. Börnert P, Koken P, Eggers H. Spiral water-fat imaging with integrated off-resonance correction on a clinical scanner. *J Magn Reson Imaging*. 2010;32:1262-1267.

33. Maeder Y, Dunet V, Richard R, Becce F, Omoumi P. Bone marrow metastases: T_2-weighted dixon Spin-Echo fat images can replace T_1-weighted Spin-Echo images. *Radiology*. 2018;286:948-959.

34. Park EH, Lee KB. Usefulness of black boundary artifact on opposed-phase imaging from turbo spin-echo two-point mDixon MRI for delineation of an arthroscopically confirmed small fracture of the lateral talar dome: a case report. *Medicine*. 2017;96:e9497.

35. You JH, Kim IH, Hwang J, Lee HS, Park EH. Fracture of ankle: MRI using opposed-phase imaging obtained from turbo spin echo modified Dixon image shows improved sensitivity. *Br J Radiol*. 2018;91:20170779.

APPENDIX A

SPLINE COEFFICIENTS

$$a_1 = \frac{4\left(3M_1T_2{}^4 - M_2T_1{}^4 + 6M_1T_1{}^2T_2{}^2 - 6M_2T_1{}^2T_2{}^2 + 10M_1T_1T_2{}^3 - 6M_2T_1{}^3T_2\right)}{T_1{}^2T_2{}^2\left(2T_1+3T_2\right)\left(T_1+T_2\right)}$$

(A1)

$$a_2 = \frac{12\left(M_2T_1{}^3 + 4M_2T_1{}^2T_2 - 4M_1T_1T_2{}^2 - M_1T_2{}^3\right)}{2T_1{}^4T_2{}^2 + 3T_1{}^3T_2{}^3}$$

(A2)

$$a_3 = \frac{4\left(M_1T_2{}^4 - 2M_2T_1{}^4 + 6M_1T_1{}^2T_2{}^2 - 4M_2T_1{}^2T_2{}^2 + 5M_1T_1T_2{}^3 - 8M_2T_1{}^3T_2\right)}{T_1{}^4T_2\left(T_1+T_2\right)\left(3T_2{}^2+2T_1T_2\right)}$$

(A3)

$$\begin{bmatrix} b_0 \\ b_1 \\ b_2 \\ b_3 \end{bmatrix} = \begin{bmatrix} a_3T_1{}^3 + a_2T_1{}^2 + a_1T_1 \\ 3a_3T_1{}^2 + 2a_2T_1 + a_1 \\ 3a_3T_1 + a_2 \\ -\left(3a_3T_1 + a_2\right)/3T_2 \end{bmatrix}$$

(A4)